

# A new interferometric study of four exoplanet host stars : $\theta$ Cygni, 14 Andromedae, $\nu$ Andromedae and 42 Draconis. $\star$

R. Ligi<sup>1</sup>, D. Mourard<sup>1</sup>, A.M. Lagrange<sup>2</sup>, K. Perraut<sup>2</sup>, T. Boyajian<sup>4\*\*</sup>, Ph. B erio<sup>1</sup>, N. Nardetto<sup>1</sup>, I. Tallon-Bosc<sup>3</sup>, H. McAlister<sup>4,5</sup>, T. ten Brummelaar<sup>4</sup>, S. Ridgway<sup>6</sup>, J. Sturmann<sup>4</sup>, L. Sturmann<sup>4</sup>, N. Turner<sup>4</sup>, C. Farrington<sup>4</sup> and P.J. Goldfinger<sup>4</sup>

<sup>1</sup> Laboratoire Lagrange, UMR 7293 UNS-CNRS-OCA, Boulevard de l'Observatoire, B.P. 4229 F, 06304 NICE Cedex 4, France.

<sup>2</sup> UJF-Grenoble1/CNRS-INSU, Institut de Plan etologie et d'Astrophysique de Grenoble, UMR 5274, Grenoble, F-38041, France

<sup>3</sup> Universit  de Lyon, 69003 Lyon : Universit  Lyon 1, Observatoire de Lyon, 9 Avenue Charles Andr , 69230 Saint-Genis Laval : CNRS, UMR 5574, Centre de Recherche Astrophysique de Lyon : Ecole Normale Sup rieure de Lyon, 69007 Lyon, France

<sup>4</sup> Georgia State University, P.O. Box 3969, Atlanta GA 30302-3969, USA

<sup>5</sup> CHARA Array, Mount Wilson Observatory, 91023 Mount Wilson CA, USA

<sup>6</sup> National Optical Astronomy Observatory, PO Box 26732, Tucson, AZ 85726, USA

Received ...; accepted ...

## Abstract

**Context.** Since the discovery of the first exoplanet in 1995 around a solar-type star, the interest in exoplanetary systems has kept increasing. Studying exoplanet host stars is of the utmost importance to establish the link between the presence of exoplanets around various types of stars and to understand the respective evolution of stars and exoplanets.

**Aims.** Using the limb-darkened diameter (LDD) obtained from interferometric data, we determine the fundamental parameters of four exoplanet host stars. We are particularly interested in the F4 main-sequence star,  $\theta$  Cyg, for which Kepler has recently revealed solar-like oscillations that are unexpected for this type of star. Furthermore, recent photometric and spectroscopic measurements with SOPHIE and ELODIE (OHP) show evidence of a quasi-periodic radial velocity of  $\sim 150$  days. Models of this periodic change in radial velocity predict either a complex planetary system orbiting the star, or a new and unidentified stellar pulsation mode.

**Methods.** We performed interferometric observations of  $\theta$  Cyg, 14 Andromedae,  $\nu$  Andromedae and 42 Draconis for two years with VEGA/CHARA (Mount Wilson, California) in several three-telescope configurations. We measured accurate limb darkened diameters and derived their radius, mass and temperature using empirical laws.

**Results.** We obtain new accurate fundamental parameters for stars 14 And,  $\nu$  And and 42 Dra. We also obtained limb darkened diameters with a minimum precision of  $\sim 1,3\%$ , leading to minimum planet masses of  $M \sin i = 5.33 \pm 0.57$ ,  $0.62 \pm 0.09$  and  $3.79 \pm 0.29 M_{\text{Jup}}$  for 14 And b,  $\nu$  And b and 42 Dra b, respectively. The interferometric measurements of  $\theta$  Cyg show a significant diameter variability that remains unexplained up to now. We propose that the presence of these discrepancies in the interferometric data is caused by either an intrinsic variation of the star or an unknown close companion orbiting around it.

**Conclusions.**

**Key words.** Techniques: high angular resolution – Instrumentation: interferometers – Methods: data analysis – Stars: fundamental parameters – Stars: individual ( $\theta$  Cyg, 14 And,  $\nu$  And, 42 Dra) –

## 1. Introduction

Many techniques have been developed during the past decade to enable the discovery of exoplanets. The radial velocity method, based on the reflex motion of the host star, is one of the most successful of these and has to date enabled the discovery of 535 planetary systems<sup>1</sup>. Most of these planets were found orbiting slowly rotating stars, late-type stars, or A giants. While A and F main sequence stars were usually avoided because of their high  $v \sin i$ , a survey of A and F main sequence stars was nonetheless recently undertaken using a specialized analysis method to look for planets around these stars, and planets were indeed found around a few F stars (Lagrange et al. 2009). Unfortunately, the possible planet configurations fitting the radial velocity (RV) data were found to be dynamically unstable. To resolve this

problem it is important to better understand the link between the presence and mass of exoplanets, the host star parameters, and the separation of the planet and host star.

Interferometric data are now able to bring additional information to bear on stellar variability and its contribution to noise in the radial velocity measurements, and can help to directly determine many of the fundamental parameters of the host stars with an accuracy of about 5% see for example (see for example Baines et al. 2009; von Braun et al. 2011). This is not only very important for deriving accurate radii for transiting planets, but also for RV planets. Understanding the link between the presence and nature of exoplanets and the fundamental parameters of the star requires sampling a large number of targets. We have started a survey with VEGA (Visible spEctroGraph and polArimeter) (Mourard et al. 2009), a visible spectro-interferometer located on the CHARA (Center for High Angular Resolution Astronomy) array at Mount Wilson, California (ten Brummelaar et al. 2005), to measure all currently accessible exoplanets stars, i.e. almost 40 targets. To build

$\star$  Based on interferometric observations with the VEGA/CHARA instrument.

\*\* Hubble Fellow

<sup>1</sup> As of December 23, 2011 (Schneider et al. 2011)

this sample, we first selected the exoplanet host stars listed in Schneider’s catalog (Schneider et al. 2011). Those stars have to be observable by VEGA, therefore we sorted out those that had a magnitude smaller than 6.5 in the V- and in the K band, and a declination higher than  $-30^\circ$ . Knowing the error on the squared visibility allowed by VEGA at medium resolution ( $\approx 2\%$ ), we can estimate the maximum and the minimum diameters for which we can obtain an accuracy of  $\approx 2\%$  taking into account the maximum and minimum baselines. We consider this accuracy as the minimum allowed to obtain sufficiently good informations on fundamental parameters of the stars and planets. Diameters included between 0.3 and 3 milliseconds of arc (mas) are sufficiently resolved to achieve this accuracy. We finally found 40 stars whose planets were discovered with the transit or RV techniques.

Interferometry is complementary to the transit method or RV measurements in determining exoplanet parameters. For instance, the transit method allows determining the exoplanet radius, while the RV method is used to detect the minimum mass. The main goal of these observations is to directly constrain these parameters, and to study the impact of stellar noise sources (e.g., spots, limb darkening) applied to these observing methods. In the long term, the results will be compared to a catalog of limb darkening laws from 3D hydro-dynamical modeling and radiative transfer. Thus, we will be able to create a catalog of measured angular diameters, and derive revised surface brightness relationships.

From October to December 2011, we obtained data on three stars of our sample : 14 And,  $\nu$  And and 42 Dra, while a fourth star  $\theta$  Cyg was observed over a longer period, from June 2010 to November 2011. We found that while the first three stars yield stable and repeatable results, there are discrepancies in the results of  $\theta$  Cyg, forcing us to study this system more carefully. New and unexplained RV variations recorded with SOPHIE and ELODIE at the Observatoire de Haute-Provence (Desort et al. 2009) provided a first clue that this star hosts either a complex planetary system, undergoes hitherto unknown variations, or has a hidden companion.

After a short introduction to the basics of interferometry, we describe in Section 3 the observations made of 14 And,  $\nu$  And and 42 Dra during the year 2011 and derive the star and planet fundamental parameters. We then compare these values to those found in the literature. In Section 4, we present the observations of  $\theta$  Cyg made during the last two years. We discuss the fundamental parameters we derived for this target in Section 5, and compare them with the previously known parameters for this star (see Table 7). We then discuss the variation of the angular diameter of  $\theta$  Cyg in Section 6 and some possible explanations of this variability.

## 2. Observations with VEGA/CHARA

### 2.1. VEGA/CHARA and visibility determination

The CHARA array hosts six one-meter telescopes arranged in a Y shape that are oriented to the east (E1 and E2), south (S1 and S2) and west (W1 and W2). The baselines range between 34 and 331 m and permit a wide range of orientations. VEGA is a spectro-interferometer working in the visible wavelengths at different spectral resolutions : 6000 and 30000. Thus, it permits the recombination of two, three or four telescopes, and a maximum angular resolution of  $\approx 0.3$  mas. Interferometry is a high angular resolution technique allowing one to study the spatial brightness distribution of celestial objects through measuring their spatial

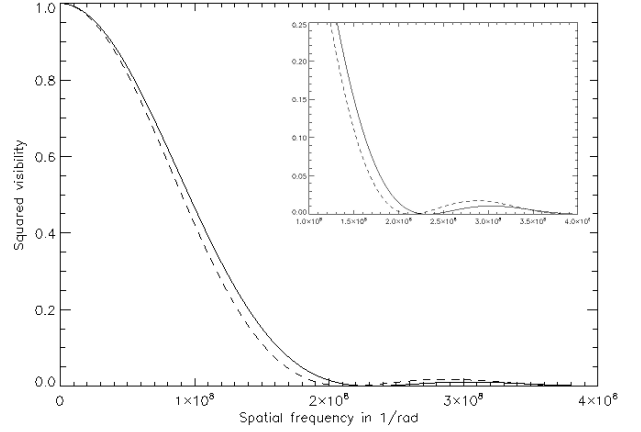


Figure 1: Squared visibility of a uniform disk (solid line) and of a limb-darkened disk (dashed line) for a star of 1.17 mas of diameter, a wavelength of 720 nm and a baseline ranging from 0 to 330 m. The LDD is sensitive close to the zero and in the second lobe of visibility, where it is higher than for a UD.

frequencies. By measuring the fringe contrast, also called visibility, one is able to determine the size of stars, thanks to the van Cittert-Zernike theorem (Born et al. 1980). The simplest representation of a star is a uniform disk (UD) of angular diameter  $\theta_{UD}$ . The corresponding visibility function is given by

$$V^2 = \left| \frac{2J_1(x)}{x} \right|^2, \quad (1)$$

where  $J_1(x)$  is the first-order Bessel function and  $x = \pi B \theta_{UD} \lambda^{-1}$ .  $B$  represents the length of the projected baseline,  $\lambda$  the wavelength of the observation. However, stars are not uniformly bright : a better representation of the surface brightness is the limb-darkened disk (LDD). The main differences between the two profiles arise close to the zero of visibility and in the second lobe, as shown in Figure 1.

The LDD is conventionally described by the function  $I_\lambda[\mu]$ , where  $\mu$  is the cosine between the normal to the surface at that point and the line of sight from the star to the observer and  $u_\lambda$  the limb darkening coefficient (Hanbury Brown et al. 1974) :

$$I_\lambda[\mu] = I_\lambda[1][1 - u_\lambda(1 - \mu)]. \quad (2)$$

A good approximation of  $\theta_{LD}$  is given by

$$\theta_{LD}[\lambda] = \theta_{UD}[\lambda] \times \left[ \frac{1 - u_\lambda/3}{1 - 7u_\lambda/15} \right]^{1/2}, \quad (3)$$

(Hanbury Brown et al. 1974).

The Claret & Bloemen (2011) coefficients are listed in tables and depend on the effective temperature and the  $\log(g)$ . We calculated that in our observing conditions, a difference of 10% on the coefficients leads to a difference of 0.65% on the LDD and of 0.33% on the  $T_{\text{eff}}$ . Using approximated coefficients is then of negligible consequence on the final parameters’ values.

Because we performed 3T observations, we obtained three calibrated squared visibility points for each observation in the observed spectral band. The systematic and statistical errors were calculated for each data point. The systematic error accounts for the influence of the estimated error on the angular diameter of the calibrators. In almost all cases, the systematic

error is negligible compared to the statistical one by a factor 10, because our diameters are small (Mourard et al. 2009). The statistical error takes into account the instrumental variations, the variations of atmospheric conditions (seeing), and vibrations of the telescopes or the delay lines. It is measured when we estimate the noise and the error on the noise.

## 2.2. Determination of the fundamental parameters

We used empirical relations to derive the fundamental parameters of the stellar and planet components. From the LDD ( $\theta_{LD}$ ) expressed in mas and the parallax ( $\pi$ ) given in second of arc, we calculated the star's linear radius ( $R$ ) and mass in the following manner. Using a simple Monte Carlo simulation, we obtain a correct estimate of the radius and its error :

$$R \pm \delta R(R_{\odot}) = \frac{\theta_{LD} \pm \delta \theta_{LD}}{9.305 \times (\pi \pm \delta \pi)}. \quad (4)$$

We then use the gravitational acceleration relation to estimate the mass :

$$\|\vec{g}\| = GM/R^2, \quad (5)$$

where  $G$  is the gravitational constant. The modulus of  $g$  is given in Table 1. The error of the mass estimate is dominated by the uncertainty in parallax. We also estimated the effective temperature using the black body law and the luminosities ( $L$ ) shown in Table 1 :

$$L = 4\pi R^2 \sigma T_{eff}^4. \quad (6)$$

Starting from the stellar masses, we use the mass function to determine the exoplanet masses and estimate its error by performing a Monte Carlo test :

$$f(m) = \frac{M_{pl}^3 \sin(i)^3}{(M_* + M_{pl})^2}, \quad (7)$$

where  $M_{pl}$  and  $M_*$  are the planet and stellar masses respectively. The results of the calculated planet masses are given in Table 6.

Given that  $M_{pl} \ll M_*$  and using Kepler's third law, we can write

$$M_{pl} \sin(i) = \frac{M_*^{2/3} P^{1/3} K (1 - e^2)^{1/2}}{(2\pi G)^{1/3}}, \quad (8)$$

where  $K$  is the velocity semi-amplitude and  $e$  the planet eccentricity.

## 3. 3T measurements of 14 And, $\nu$ And and 42 Dra

### 3.1. VEGA observations

In 2011, we observed two giant stars, 42 Dra (K1.5III: Döllinger et al. (2009)) and 14 And (K0III: Sato et al. (2008)), and one main-sequence star,  $\nu$  And (F9V: Fuhrmann et al. (1998)). The observations provided measurements close to the zero or up to the second lobe of squared visibility.

14 And (HD221345, HIP116076, HR8930) hosts one exoplanet of minimum mass  $M_2 \sin i = 4.8M_J$  discovered in 2008, and it has also been shown that this star does not exhibit measurable chromospheric activity (Sato et al. 2008). The general properties of this star are given in Table 1.

Table 1: Coordinates and parameters of the three host stars 14 And,  $\nu$  And and 42 Dra. References from <sup>(a)</sup>Sato et al. (2008) : <sup>(b)</sup>Fuhrmann et al. (1998) : <sup>(c)</sup>Döllinger et al. (2009) : <sup>(d)</sup>van Leeuwen (2007) : <sup>(e)</sup>Butler et al. (1999) : <sup>(f)</sup>Baines et al. (2010).

Parameter	14 And	$\nu$ And	42 Dra
RA (J2000)	23:31:17.4	01:36:47.8	18:25:59.14
Dec (J2000)	+39° 14' 10"	+41° 24' 20"	+65° 33' 49"
Stellar type	K0III <sup>(a)</sup>	F9V	K1.5III <sup>(c)</sup>
V mag	5.225	4.10	4.833 <sup>(c)</sup>
K mag	2.331	2.86	2.085
$M_V$	0.67 <sup>(a)</sup>	3.44±0.02 <sup>(b)</sup>	-0.09±0.04 <sup>(c)</sup>
$\nu \sin i$ [km/s]	2.60 <sup>(a)</sup>	9.5±0.8 <sup>(b)</sup>	
$T_{eff}$ [K]	4813±20 <sup>(a)</sup>	6107±80 <sup>(b)</sup>	4200±70 <sup>(c)</sup>
Parallax [mas]	12.63±0.27 <sup>(d)</sup>	74.12±0.19 <sup>(d)</sup>	10.36±0.20 <sup>(d)</sup>
Mass [ $M_{\odot}$ ]	2.2 <sup>+0.1</sup> <sub>-0.2</sub> <sup>(a)</sup>	1.27±0.06 <sup>(b)</sup>	0.98±0.05 <sup>(c)</sup>
log g	2.63±0.07 <sup>(a)</sup>	4.01±0.1 <sup>(b)</sup>	1.71±0.05 <sup>(c)</sup>
[Fe/H]	-0.24±0.03 <sup>(a)</sup>	0.09±0.006 <sup>(b)</sup>	-0.46±0.05 <sup>(c)</sup>
L [ $L_{\odot}$ ]	58 <sup>(a)</sup>	3 <sup>(e)</sup>	149.7±15.3 <sup>(f)</sup>

$\nu$  And (HD9826, HIP7513, HR458) is a bright F star that has undergone numerous spectroscopic investigations (Fuhrmann et al. 1998, and references therein). Four exoplanets are known to orbit around it: they were discovered between 1996 and 2010 (Schneider et al. 2011; Butler et al. 1999; Lowrance et al. 2002; Curiel et al. 2011).

42 Dra (HD170693, HIP90344, HR6945) is an intermediate-mass giant star around which a  $3.88 \pm 0.85M_J$  exoplanet has recently been discovered (Döllinger et al. 2009).

Table 2: Parameters of the calibrators used for 14 And,  $\nu$  And and 42 Dra. The value of the equivalent uniform disk  $\theta_{UD}$  is given at 700nm (Bonneau et al. 2006).

#	Name	Spectral Type	$m_V$	$m_K$	$\theta_{UD}$ [mas]
1	HD 211211	A2Vnn	5.71	5.63	0.20±0.01
2	HD 1439	A0IV	5.87	5.86	0.18±0.01
3	HD 14212	A1V	5.31	5.27	0.24±0.02
4	HD 187340	A2III	5.90	5.71	0.21±0.02

Observations of these three exoplanet host stars were made in October and November 2011 with the E1E2W2 triplet. The data processing and the results analysis were presented in Subsection 2.1. We used the calibrators HD211211 (*cal1*) and HD1439 (*cal2*) for 14 And, HD14212 (*cal3*) for  $\nu$  And and HD187340 (*cal4*) for 42 Dra (Table 2). They were found using the SearchCal utility<sup>2</sup> developed by the JMMC (Bonneau et al. 2006). It gives, among other parameters, the stellar magnitude in the V and K bands, the spectral type, and also an estimate of the angular diameter along with the corresponding error. Angular diameters are determined by surface-brightness versus color-index relationships. We used the  $V/(V - K)$  polynomial relation given by Bonneau et al. (2006). Its accuracy of 7% is the highest concerning the color-index polynomial fits. We mainly observed with the three telescope (3T) configuration, but sometimes the conditions only allowed for 2T measurements (Table 3). VEGA data are recorded as blocks of 1000 frames each of 15 milliseconds of exposure time. The observations of the targets were 30 minutes long (60 blocks), and those of the calibrators were 10 to 20 minutes long (20 or 40 blocks). The data were recorded at

<sup>2</sup> Available at <http://www.jmmc.fr/searchcal>

Table 3: Journal of the observations of 14 And,  $\nu$  And and 42 Dra. RJD is the reduced Julian day. The projected baseline is given by baseline (in meters) and PA in degree.  $V^2$  is the calibrated squared visibility, the error of the squared visibility includes the statistical and systematic errors. All measurements use a band of 15nm around 707.5nm, except for the last observation of 42 Dra, which was centered around 732.5nm. In most cases (\*), CLIMB data in K band are also available.

Star	RJD	Seq	Base	PA	$V^2$
14 And	55855.4	1T1	66	-123.4	0.306±0.022
			222	-118.7	0.004±0.032
	55849.68*	1T1	104	109.1	0.047±0.015
			153	-108.2	0.012±0.016
			244	-93.2	0.008±0.017
	55847.77*	1T1	65	-134.1	0.321±0.016
			154	-127.2	0.020±0.008
	55847.72*	1T2	66	-122.9	0.420±0.022
			156	-118.1	0.039±0.012
	$\nu$ And	55883.74*	3T3	66	-131.3
156				-124.46	0.007±0.009
221				-126.4	0.007±0.009
55855.69*		3T3	92	131	0.277±0.011
			95.9	124.2	0.245±0.009
55855.72*		3T3	107	89.9	0.226±0.012
55855.85*		3T	107	89.9	0.226±0.012
			156	-120.2	0.437±0.027
55854.78*		3T3	151	-113.5	0.000±0.007
			221	-115.5	0.023±0.011
	222		-115.5	0.023±0.011	
42 Dra	55883.63*	4T4	66	169.5	0.100±0.015
			66	-164.9	0.086±0.007
	55854.63*	4T4	66	-164.9	0.111±0.009
			156	-159.0	0.000±0.006
55854.63*	4T4	222	-160.7	0.006±0.011	

medium spectral resolution ( $R = 6000$ ) and the data processing used 15 nm wide channels in the continuum of the red spectrum. We alternated the calibrators and target using the standard sequence *Cal-Target-Cal*, which provides a better estimate of the transfer function during the observations of the target. We know (Mourard et al. 2009) that, under correct seeing conditions, the transfer function of VEGA/CHARA is stable at the level of 2% for more than one hour. This has been checked in all our data set, and bad sequences were removed. We used the CLIMB beam combiner operating in the near-infrared as a 3T fringe tracker (Sturmann et al. 2010) to stabilize the optical path differences during the long integrations.

### 3.2. Fundamental parameters of stars and planets

Because our data sets are covering many frequencies in the second lobe of the visibility function, we decided to fix the LDD coefficient and to adjust the diameter only. We used Claret & Bloemen (2011) tables.

#### – 14 And

This star is well-fitted by a limb-darkened diameter model that provides a  $\chi^2_{\text{reduced}}$  of 2.8 (see Figure 2). It is obtained with the Claret coefficient  $u_\lambda = 0.700$ , defined by the effective temperature and the  $\log(g)$  given in Table 1. It follows a LDD of  $1.51 \pm 0.02$  mas. Baines et al. (2009) found an LDD of  $1.34 \pm 0.01$  mas for 14 And, which is smaller by  $\sim 10\%$  than the one we found with VEGA. But we recorded the data in the V band, whereas their values were recorded in the K band. Sato et al. (2008) found that 14 And’s exoplanet minimum mass is  $M_{\text{pl}} \sin(i) = 4.8M_{\text{Jup}}$ , which is close to our re-

sult (see Table 6), but was derived from radial velocity data, which induces a different bias.

#### – $\nu$ And

The data points obtained at low spatial frequency are slightly lower than the LDD model. This explains the higher  $\chi^2_{\text{reduced}}$  than for the other stars, which equals 6.9 (Figure 2). Then, we obtained  $\theta_{\text{LD}} = 1.18 \pm 0.01$  mas using  $u_\lambda = 0.534$ .  $\nu$  And was observed by van Belle & von Braun (2009) with the Palomar Testbed Interferometer (PTI), who estimated its LDD to be  $1.02 \pm 0.06$  mas. Baines et al. (2008) found a higher diameter with CHARA/CLASSIC (McAlister et al. 2005):  $1.11 \pm 0.01$  mas. However, it appears that, due to the dispersion in their measurements, the value of their error bars could be underestimated. In our case, the formal uncertainty is also very small but the high value of the  $\chi^2_{\text{reduced}}$  indicates a poor adjustment by this simple model. No value is consistent with the respective other, ours being separated from Baines et al. (2008)’s by more than  $5\sigma$ . More observations are definitively necessary to improve the accuracy and reliability of these measurements.

However, the minimum masses of  $\nu$  And’s exoplanets are consistent with those calculated by Curiel et al. (2011) and Wright et al. (2009), but remain lower by  $\simeq 10\%$  on average, when we use the orbital periods, semi-amplitudes, and eccentricities they both give (Table 6).

#### – 42 Dra

The  $\chi^2_{\text{reduced}}$  we obtained for 42 Dra is our lowest: 0.2. The LDD model perfectly fits the data points. This leads to a  $\theta_{\text{LD}}$  of  $2.12 \pm 0.02$  mas with a Claret coefficient of  $u_\lambda = 0.725$ . Baines et al. (2010) found a similar LDD to ours for 42 Dra:  $2.04 \pm 0.04$  mas. Given the few studies of this stars, this additional measurement brings a new accurate confirmation of the diameter. Concerning the planet’s fundamental parameter, we found a similar  $M_{\text{pl}} \sin(i)$  to that calculated by Döllinger et al. (2009) (see Table 6).

Because CLIMB works in the K band, we used the corresponding Claret coefficients to estimate the LDD in this spectral band, resulting in  $u_\lambda = 0.321$ ,  $u_\lambda = 0.247$  and  $u_\lambda = 0.353$  for 14 And,  $\nu$  And and 42 Dra, respectively. In each case we used the effective temperature and the  $\log(g)$  given in Table 1. Because CLIMB data are not very sensitive to limb darkening, because of the relatively low spatial frequencies and the fact that there is less limb darkening in K band, we used the visible coefficient for the global (VEGA+CLIMB) analysis. Although the  $\chi^2_{\text{reduced}}$  becomes slightly lower when including CLIMB data (Table 4), the final results for the LDD are not changed, as expected because of the lower precision of the CLIMB visibilities and the lower influence on the diameter of the low spatial frequencies. The global results (VEGA+CLIMB) are thus the same as those obtained with VEGA only. The CLIMB data did not bring any improvements for this study.

## 4. Interferometric observations of $\theta$ Cygni with VEGA/CHARA

### 4.1. $\theta$ Cygni

$\theta$  Cyg (HD185395,  $d = 18.33 \pm 0.05$  pc, Table 7) is an F4V star with an M-dwarf companion of  $0.35 M_\odot$  orbiting at a projected separation of  $2''$  ( $\simeq 46$  AU) and with a differential magnitude of 4.6 mag in the H band. Using the data provided by Delfosse et al. (2000), this  $dM$  translates into 7.9 mag

Table 6: Calculated exoplanets masses of 14 And,  $\nu$  And and 42 Dra from interferometric data and comparison with previous work (<sup>(a)</sup>Sato et al. 2008; <sup>(b)</sup>Curiel et al. 2011; <sup>(c)</sup>Döllinger et al. 2009).

Planet	$P_{\text{orb}}[\text{days}]$	K [ $m.s^{-1}$ ]	e	$M_{\text{pl}} \sin(i)[M_{\text{Jup}}]$	
				This work	Previous work
14 And b	185.84±0.23	100.0±1.3	0	5.33±0.57	4.8 <sup>(a)</sup>
$\nu$ And b	4.62±0.23	70.51±0.45	0.022±0.007	0.62±0.09	0.69±0.04 <sup>(b)</sup>
$\nu$ And c	241.26±0.64	56.26±0.52	0.260±0.079	1.80±0.26	1.98±0.19 <sup>(b)</sup>
$\nu$ And d	1276.46±0.57	68.14±0.45	0.299±0.072	3.75±0.54	4.13±0.29 <sup>(b)</sup>
$\nu$ And e	3848.86±0.74	11.54±0.31	0.0055±0.0004	0.96±0.14	1.06±0.28 <sup>(b)</sup>
42 Dra b	479.1±6.2	112.5	0	3.79±0.29	3.88±0.85 <sup>(c)</sup>

Table 4: Summary of the 14 And,  $\nu$  And and 42 Dra limb-darkened diameters (mas) calculated for VEGA data, CLIMB data and both instruments.

Star	VEGA		CLIMB		VEGA+CLIMB	
	$\theta_{\text{LD}}$	$\chi^2$	$\theta_{\text{LD}}$	$\chi^2$	$\theta_{\text{LD}}$	$\chi^2$
14 And	1.51±0.02	2.8	1.30±0.13	1.5	1.50±0.02	2.1
$\nu$ And	1.18±0.01	6.9	0.96±0.16	0.8	1.17±0.01	4.6
42 Dra	2.12±0.02	0.2	2.10±0.27	0.4	2.12±0.02	0.3

Table 5: Summary of the fundamental parameters of 14 And,  $\nu$  And and 42 Dra calculated using VEGA interferometric data.  $\theta_{\text{LD}}$  is the limb-darkened diameter in mas. The radius and mass are given in solar units and  $T_{\text{eff}}$  is given in K.

Star	Radius	Mass	$T_{\text{eff}}$
14 And	12.82±0.32	2.60±0.42	4450±78
$\nu$ And	1.70±0.02	1.12±0.25	5819±78
42 Dra	22.04±0.48	0.92±0.11	4301±71

in the V band (Desort et al. 2009). More recently, Roberts (2011) published adaptive optics (AO) data obtained with the AEOS telescopes in 2002, and reported a differential magnitude in the Bessel I-band of  $5.89 \pm 0.089$  and a separation of  $2.54''$ . This is compatible with a contrast of  $\approx 7$  at the V band. Spectroscopic data of  $\theta$  Cyg collected with ELODIE and SOPHIE at the Observatoire de Haute-Provence (OHP) revealed quasi-periodical radial velocity variations with a period of approximately 150 days. No known stellar variation modes can explain such long-term, high-amplitude RV variations. They were tentatively attributed to the presence of more than two exoplanets, possibly interacting with each other. However, this explanation was not only unsatisfactory because it is dynamically unstable, but also because it did not straightforwardly explain a peak observed in the periodogram of the bisector velocity span at  $\approx 150$  days. Clearly, the data at hand were not sufficient to fully understand this complex system.

Our interferometric observations in the visible wavelengths have both high spatial and spectral resolution and help us probe the same domain as these spectroscopic results. Furthermore, we obtained measurements very close to the first zero of the visibility function (see Section 2.1), which allows accurate angular diameter determination and the possible identification of stellar pulsations. As a Kepler target, photometric observations were obtained in 2010 and solar-like oscillations were detected (Guzik et al. 2011). These observations imply the possible presence of  $\gamma$  Dor gravity modes, which are generally present in early-F spectral type stars. If these oscillations are confirmed,

Table 7:  $\theta$  Cyg, coordinates and parameters. References from <sup>(a)</sup>Desort et al. (2009); <sup>(b)</sup>Boyajian et al. (2012); <sup>(c)</sup>van Belle et al. (2008); <sup>(d)</sup>Guzik et al. (2011); <sup>(e)</sup>Ersparmer & North (2003); <sup>(f)</sup>van Leeuwen (2007)

Coordinates		
RA (J2000)	19 : 36 : 26.5	
Dec (J2000)	+ 50° 13' 16''	
Stellar parameters		Values
Stellar type	F4V	
V mag	4.50±009	
K mag	3.5±0.296	
$M_V$	3.14	
$\nu \sin i$ [km/s]	7	
$T_{\text{eff}}$ [K]	6745 <sup>(a)</sup>	6381±65 <sup>(b)</sup>
Distance [pc]	18.33±0.05	
Parallax [mas]	54.54±0.15 <sup>(f)</sup>	
Radius [ $R_{\odot}$ ]	1.70±0.03 <sup>(b)</sup>	
Mass [ $M_{\odot}$ ]	1.38±0.05 <sup>(a)</sup>	1.34±0.01 <sup>(b)</sup>
Age [Gyr]	1.5 $\pm_{-0.7}^{+0.6}$ <sup>(a)</sup>	2.8±0.2 <sup>(b)</sup>
log g	4.2 <sup>(e)</sup>	
[Fe/H]	-0.08 <sup>(a)</sup>	-0.04 <sup>(b)</sup>
log L [ $L_{\odot}$ ]	0.63±0.003 <sup>(d)</sup>	4.265±0.090 <sup>(b)</sup>

$\theta$  Cyg would be the first star to show signs of both solar-like and  $\gamma$  Dor oscillations (Guzik & Mussack 2010, and references therein).

#### 4.2. VEGA observations

We performed nine observations of  $\theta$  Cyg with VEGA from June 2010 to October 2011. We used the three-telescope capabilities of the instrument (Mourard et al. 2011), using the telescope combinations E1E2W2, W1W2E2 and W1W2E1 triplets of the CHARA array.

Three stars were used as calibrators: HD177003 (*cal1*), HD177196 (*cal2*) and HD203245 (*cal3*), whose parameters are summarized in Table 8.

Table 8: Calibrators used for  $\theta$  Cyg observations. The value of the equivalent uniform disk  $\theta_{\text{UD}}$  is given at 700nm.

#	Name	Spectral Type	$m_V$	$m_K$	$\theta_{\text{UD}}[\text{mas}]$
1	HD 177003	B2.5IV	5.37	5.89	0.13±0.01
2	HD 177196	A7V	5.01	4.51	0.43±0.03
3	HD 203245	B6V	5.74	6.10	0.14±0.01

If the target was observed only once during a night, the observing sequence was *Cal1-Target-Cal1*, each calibrator observation being 20 to 40 blocks of 1000 frames long, depend-

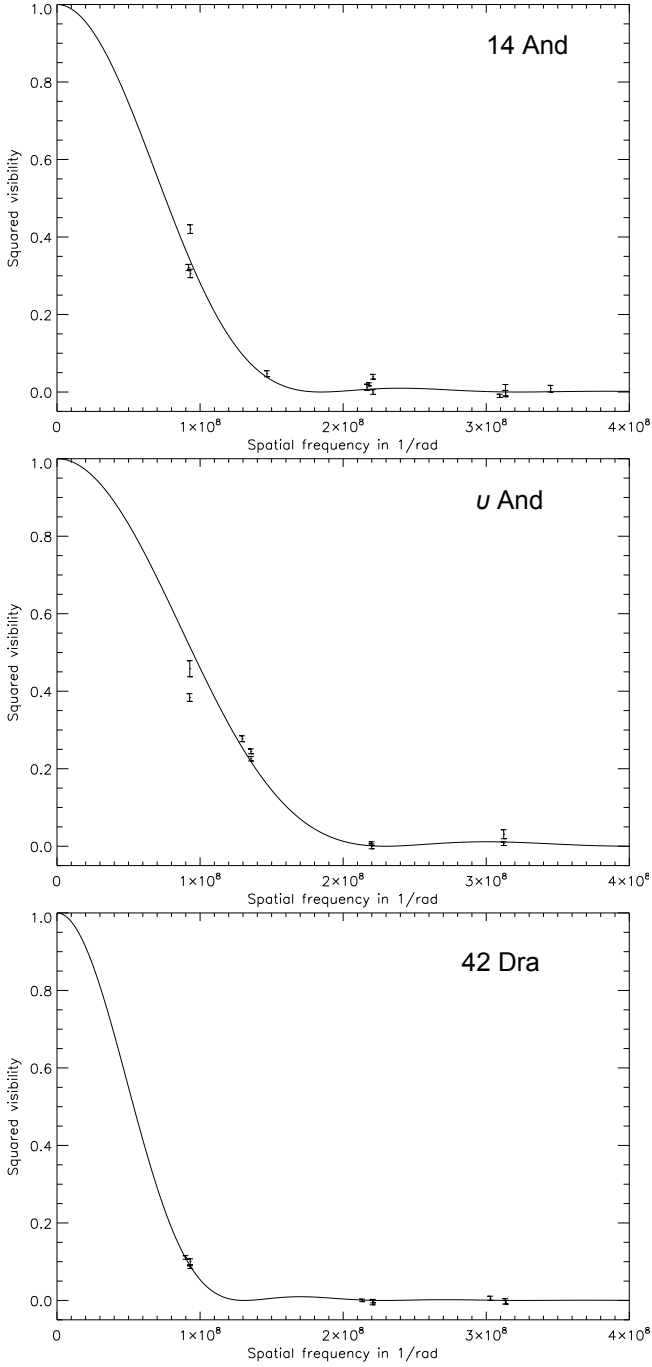


Figure 2: Squared visibility of 14 And (top),  $\nu$  And (middle) and 42 Dra (bottom) versus spatial frequency [1/rad] for VEGA data points. The solid line is the model of the limb-darkened angular diameter provided by the LITpro software.

ing on the magnitude, that is between about 10 and 20 minutes, while each target observation was 60 blocks of 1000 frames long, or about 30 minutes. When the target was observed twice, the observing sequence was either *Cal1-Target-Cal2-Target-Cal2*, or *Cal2-Cal1-Target-Cal1-Cal2-Target-Cal3*. The data were recorded at medium spectral resolution and the data processing was performed on 15 to 30 nm wide channels in the continuum. The calibrated visibilities are presented in Table 9. To take into account the variation of the spatial frequency due to the width of the spectral band (bandwidth smearing effect), we calculated its effect on the visibility. We found it to be

Table 9: Journal of the observations of  $\theta$  Cyg. RJD is the reduced Julian day,  $\lambda_0$  is the central wavelength in nm,  $\Delta\lambda$  is the width in nm of the analyzed spectral band. Column 4 (entitled Seq) indicates the observing and calibration strategy, with the target (T) and the associated calibrator (1, 2 or 3). The projected baseline is given by Base (in meter) and PA (in degree).  $V^2$  is the calibrated squared visibility with a total error including statistical and systematic errors. They all represent 3-T measurements.

RJD	$\lambda_0$	$\Delta\lambda$	Seq	Base	PA	$V^2$
55849.62	707.5	15	1T3	106	84.6	$0.534 \pm 0.022$
				156	-131.9	$0.237 \pm 0.015$
				249	-134.5	$0.028 \pm 0.021$
55848.62	707.5	15	1T3	106	83.9	$0.502 \pm 0.020$
				156	-132.6	$0.192 \pm 0.007$
				249	-135.5	$0.048 \pm 0.014$
55826.67	737.0	14	T1	66	-139.1	$0.801 \pm 0.038$
				156	-132.3	$0.229 \pm 0.016$
				221	-134.3	$0.054 \pm 0.028$
55826.74	737.0	14	1T	65	-157.3	$0.822 \pm 0.036$
				152	-150.8	$0.286 \pm 0.014$
				216	-152.7	$0.017 \pm 0.019$
55805.75	737.5	15	1T1	65	-143.9	$0.885 \pm 0.023$
				155	-137.2	$0.236 \pm 0.011$
				220	-147.7	$0.039 \pm 0.022$
55803.77	737.5	15	3T3	103	75.6	$0.549 \pm 0.011$
				154	-141.3	$0.195 \pm 0.012$
				245	-146.6	$0.040 \pm 0.018$
55774.73	709.5	15	1T1	106	109.9	$0.481 \pm 0.015$
				153	-107.4	$0.130 \pm 0.010$
				108	95.1	$0.451 \pm 0.015$
55722.93	735.0	20	21T12	156	-121.3	$0.166 \pm 0.009$
				106	82.1	$0.493 \pm 0.013$
				155	-134.5	$0.181 \pm 0.008$
55722.98	735.0	20	12T3	64	-167.3	$0.813 \pm 0.016$
				150	-161.0	$0.169 \pm 0.009$
				214	-162.9	$0.027 \pm 0.019$
55486.71	670.0	20	1T1	64	179.7	$0.928 \pm 0.020$
				148	-174.0	$0.166 \pm 0.010$
				156	-127.0	$0.152 \pm 0.013$
55486.74	670.0	20	1T1	222	-129.0	$0.012 \pm 0.010$
				66	-133.8	$0.788 \pm 0.028$
				156	-127.0	$0.152 \pm 0.013$
55370.92	715.0	30	T2	65	-148.4	$0.802 \pm 0.030$
				154	-141.7	$0.221 \pm 0.019$
				219	-143.7	$0.039 \pm 0.015$

totally negligible (variation lower than the error bars of the measurements, Mourard et al. 2009). Moreover, the data processing was performed with the same parameters for one observing sequence and effects such as these will largely calibrate out. For most of these observations, interferometric data in the infrared wavelength (K band) were also recorded with CLIMB, which was used as a 3T group delay fringe tracker (Sturmann et al. 2010). However, the baselines chosen for VEGA were too small for this object to be resolved in K band and the CLIMB data were not used in the final analysis.

## 5. Determination of $\theta$ Cygni's fundamental parameters

### 5.1. Determination of the limb-darkened diameter

For almost all observations including the E1E2 baseline, we obtained a  $\chi^2_{\text{reduced}}$  larger than 2. The E2 telescope is known to present instabilities, like vibrations and delay line cart problems. Those points are therefore more dispersed than those at

higher spatial frequencies, as shown in Figure 3 and Table 11, and the value of  $\chi^2_{\text{reduced}}$  is mostly dominated by these points. In a first analysis, we have considered all data points. We used the LitPro software<sup>3</sup> (Tallon-Bosc et al. 2008) and obtained a mean UD equivalent diameter of  $0.726 \pm 0.003$  mas. The  $\chi^2_{\text{reduced}}$  of the model fitting is equal to 8.4, which clearly indicates dispersion in the measurements or possible variations of the diameter from night to night. This will be investigated in Sect. 6. We also tested a linear limb-darkened (LD) disk model with a coefficient  $u_\lambda$  as defined by Hanbury Brown et al. (1974). Unfortunately, the data quality at low-visibility levels is not sufficient for a correct  $u_\lambda$  determination. For a more detailed analysis, we decided to fix the linear LD coefficient in the LitPro software. With  $T_{\text{eff}} = 6745$  K and  $\log(g) = 4.2$ , we used the value of the Claret coefficients (Claret & Bloemen 2011) given for the R, I and J bands, and deduced by extrapolation the value at the observing wavelengths (715 and 670 nm). We found  $u_{670\text{nm}} = 0.510$  and  $u_{715\text{nm}} = 0.493$ , and finally took the mean value 0.5. The adjustment of the whole data set (see Figure 3) gives the value  $\theta_{\text{LD}} = 0.760 \pm 0.003$  mas, with a reduced  $\chi^2_{\text{reduced}}$  equal to 8.5.

Our final value is consistent with the diameter estimated by van Belle et al. (2008) with spectral energy distribution based on photometric observations : they found  $\theta_{\text{LD}} = 0.760 \pm 0.021$  mas. Boyajian et al. (2012) observed this star in 2007 and 2008 with the CHARA CLASSIC beam combiner operating in the K band, and found  $\theta_{\text{LD}} = 0.845 \pm 0.015$  mas and  $\theta_{\text{LD}} = 0.861 \pm 0.015$  mas, which is much larger than ours. We will return to this point in Sect.6.

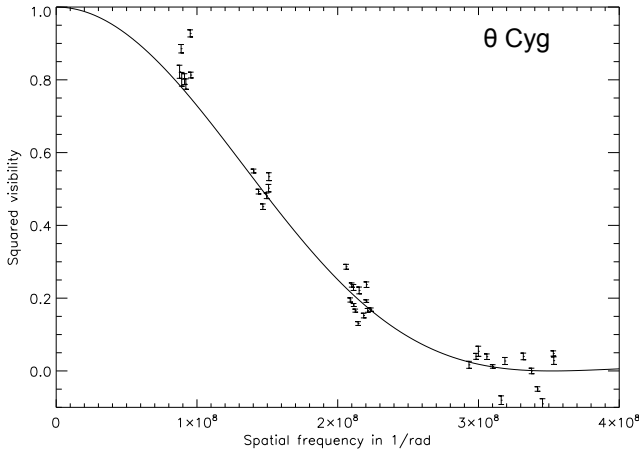


Figure 3: Squared visibility of  $\theta$  Cyg as a function of the spatial frequency [1/rad] for all data points recorded in 2010 and 2011 by VEGA (3T configuration). The solid line is the squared visibility function for a linear limb-darkened disk model with a diameter of 0.76 mas and a limb-darkening coefficient of 0.5, obtained with LITpro software.

As previously stated, the CLIMB measurements have large scatter and are at much lower spatial frequencies than the VEGA data. They provide a LDD equal to  $\theta_{\text{LD}} = 0.654 \pm 0.090$  mas, with a  $\chi^2_{\text{reduced}} = 1.86$ , obtained with a Claret coefficient of 0.22 corresponding to the K band. When combining the CLIMB and VEGA data, the diameter remains the same, except that the  $\chi^2_{\text{reduced}}$  decreases to 5.3. This is because of the large error bars obtained for CLIMB data at high frequencies, which do not con-

Table 10: Table summarizing  $\theta$  Cyg’s fundamental parameters calculated with the interferometric data.

Stellar parameters	Value±Error
LD diameter [mas]	0.760±0.003
Radius [ $R_\odot$ ]	1.503±0.007
Mass [ $M_\odot$ ]	1.32±0.14
$T_{\text{eff}}$ [K]	6767±87

Table 11: Values of the mean  $\theta_{\text{LD}}$  per night for  $\theta$  Cyg and the corresponding  $\chi^2_{\text{reduced}}$ .

Epoch	Baselines	$\theta_{\text{LD}}$	$\phi \text{ mod } 150$	$\chi^2_{\text{reduced}}$
55849.62	W2W1E2	0.700±0.011	0.33	0.700
55848.62	W2W1E2	0.744±0.007	0.32	5.698
55826.67	E2E1W2	0.721±0.009	0.18	1.12
55805.75	E2E1W2	0.727±0.010	0.04	7.749
55803.77	W2W1E2	0.759±0.008	0.03	5.936
55774.73	W2W1E2	0.807±0.010	0.83	13.9
55722.93	W2W1E2	0.793±0.006	0.49	0.664
55486.71	E2E1W2	0.744±0.007	0.91	23.2
55370.92	E2E1W2	0.764±0.010	0.14	2.468

strain  $\theta$  Cyg’s LDD at all, although they reduce the  $\chi^2_{\text{reduced}}$ . For  $\theta$  Cyg, the scatter affects all measurements.

## 5.2. Determination of fundamental parameters

The radius and the mass of  $\theta$  Cyg were estimated using Equations 4 and 5. We took  $\pi = 54.54 \pm 0.15$  mas according to van Leeuwen (2007).  $\theta$  Cyg’s radius is then  $R = 1.503 \pm 0.007 R_\odot$ . The final uncertainty is equally due to errors in the parallax and the angular diameter. This results in a mass of  $1.32 \pm 0.14 M_\odot$  and locates  $\theta$  Cyg between the two lines representing the evolutionary tracks of Figure 4 in the model of Guzik et al. (2011). Finally, the effective temperature was calculated using Equation 6 and the luminosities shown in Table 7. The errors were calculated using the Monte Carlo method. This results in  $T_{\text{eff}} = 6767 \pm 87$  K, which is also consistent with the value given by Desort et al. (2009). Boyajian et al. (2012) found a lower  $T_{\text{eff}}$  of  $6381 \pm 65$  K mostly due to a larger limb-darkened diameter (see Table 7). Table 10 summarizes the results based on our interferometric measurements.

## 6. Discussion

We have seen in the previous section that the scatter of measurements for  $\theta$  Cyg is larger than for the three other targets. It remains then to understand these variations. Table 11 shows the night-to-night variations in the LDD of  $\theta$  Cyg. The UD and LD models do not fit these results very well, as indicated by the generally high value of  $\chi^2_{\text{reduced}}$ . Boyajian et al. (2012)’s CLASSIC data obtained between 2007 and 2008 also show some discrepancies in their visibility curve fitted with a UD model. This introduces the possibility of either an additional companion, or stellar variations around  $\theta$  Cyg. The night-by-night observing strategy we employed so far was not optimized for the investigation of binarity but for the measurement of fundamental parameters. Thus, the UV coverage (Figure 4), which represents the support of the spatial frequencies measured by the interferometer, does not constrain on the position of an hypothetical companion very well.

<sup>3</sup> Available at <http://www.jmmc.fr/litpro>

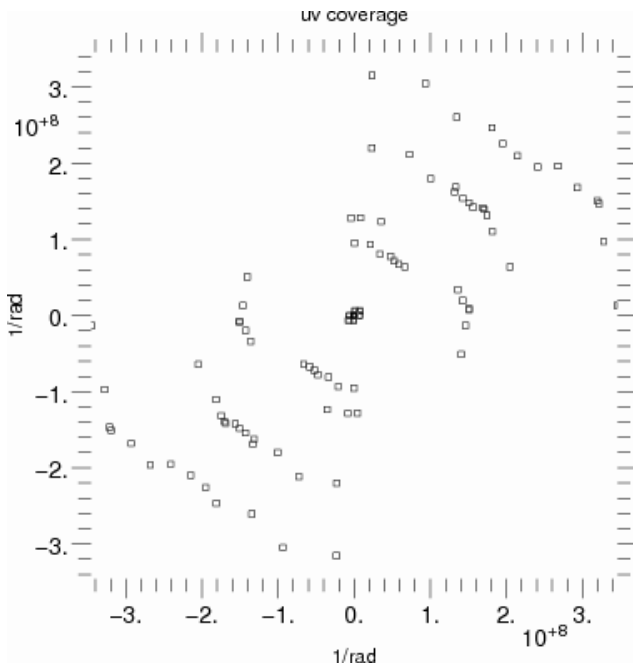


Figure 4: UV coverage of the baselines used during  $\theta$  Cyg observations from 2010 to 2011.

### 6.1. Stellar variations

Because  $\theta$  Cyg’s radial velocity is suspected to have a 150-day period (Desort et al. 2009), we studied a possible correlation between the variation of the diameter and this periodic behavior of the radial velocities. Figure 5 represents the individual angular diameter plotted as a function of a phase ( $\phi$ ) corresponding to the reduced Julian day *modulo* the spectroscopic period of 150 days. This figure highlights a possible variation with an amplitude of  $\sim 13\%$  in diameter peak to peak. Solar-like oscillations lead to lower variations in amplitude than that, but Cepheid stars show similar-sized pulsations. According to  $\theta$  Cyg’s luminosity, however, it is not bright enough to be classified as a Cepheid. Moreover, a Cepheid’s light curve presents much larger amplitude variations than  $\theta$  Cyg’s (Figure 1 in Guzik et al. 2011). Its luminosity and temperature would instead locate it near the instability branch of the HR diagram, identifying it as a  $\delta$  Scuti or  $\gamma$  Dor star, which are also A- or F- type stars.

This last possibility is also mentioned by Guzik et al. (2011), who proposed two different models that could show evidence for  $\gamma$  Dor pulsations, but they only allowed  $l = 1$  or  $l = 2$  unstable g-modes. Their light curve does not reveal the typical  $\gamma$  Dor frequencies around  $11 \mu\text{Hz}$ , which are specific for these pulsations, though they do mention that these could be overshadowed by the granulation noise. Moreover,  $\gamma$  Dor oscillations have been found in many Kepler sources without much ambiguity because they show obvious evidence for this type of pulsation (Tkachenko et al. 2012). Also, the RV measurements published in Desort et al. (2009) do not reveal high-amplitude and high-frequency (hours to days) RV variations typical of  $\gamma$  Dor stars or  $\delta$  Scuti stars.

Finally, we note that if the 150-day period RV variations were due to diameter variations, these diameter variations would be unrealistically large, much larger than those observed, and very significant photometric variations should have been detected by Kepler.

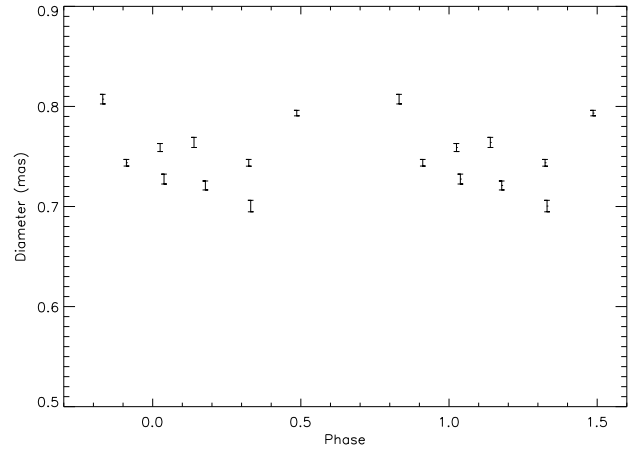


Figure 5: Individual angular diameter measurements of  $\theta$  Cyg according to the phase. The phase is proportional to the reduced Julian day *modulo* 150, as the radial-velocity period is expected to be.

We therefore conclude that stellar variations do not explain the observed features in a satisfactory manner. We therefore consider the possibility of an unseen stellar companion for  $\theta$  Cyg, and see how the present interferometric data can help to test such a scenario.

### 6.2. An additional companion?

The known M-type companion to  $\theta$  Cyg clearly does not affect our visibilities, because of the large separation in position (2 seconds of arc) and the large difference in magnitude (around 7). Any instrument hosted by the CHARA array and used in the same conditions as we did (e.g., medium resolution for VEGA) has an interferometric field of view much smaller than the telescopes’ Airy spot, i.e.  $\approx 0.1$  second of arc. This means that any object located beyond this field does not interfere, but could create a photometric background that disrupts the visibility of the target if it is located in the entrance field of the instrument. In our case, the  $dM$  in the V band gives a very small contribution to this background, much lower than the error bars ( $\approx 1\%$ ). We therefore consider the presence of a second and much closer companion. The lower limit of detection allowed by adaptive optics (AO) is at about the diffraction limit of PUEO on the CFHT, i.e. around 100 mas for low-contrast binaries. Accordingly, a companion whose position is closer in than this limit would not be seen in AO direct imaging. However, given our current accuracies in visibility measurements, it could be detected by interferometric instruments if its flux contribution is higher than 2%. Because  $\theta$  Cyg is not classified as SB2, such a flux ratio would imply a pole-on bound system or a visual unbound binary.

This last possibility has been considered, but is difficult to confirm. No objects are located close to  $\theta$  Cyg in the background, except for  $\theta$  Cyg-B, which could have moved closer to the main star over the years. As said by Desort et al. (2009), the differential magnitude between the two bound stars in the V band is 7.9 mag and 4.6 mag in the H band. Thus, we can expect a  $dM$  of  $\sim 3$  mag in the K band, which would make it observable with CLASSIC. A rough estimate of the orbit of  $\theta$  Cyg-B based on the data published by Desort et al. (2009) shows that at the epoch of the interferometric observations, the separation is still larger than



Table 12: Comparison between a UD model and a model with a companion for VEGA and CLASSIC data. For each set of simulation, this table gives the orbital parameters obtained with the minimum  $\chi^2_{\text{reduced}}$  and the corresponding flux.

Epoch	UD model		Binary model			
	$\theta_{\text{UD}}$ [mas]	$\chi^2_{\text{reduced}}$	$\rho$ [mas]	PA [ $^\circ$ ]	Flux %	$\chi^2_{\text{reduced}}$
<b>VEGA</b>						
55849.62	0.670	0.8	7.1	72.2	15	0.9
55848.62	0.710	5.7	11.1	234.7	15	5.9
55826.67	0.689	1.1	50.5	75.2	15	1.0
55805.75	0.695	7.6	10.3	10.0	15	11.5
55803.77	0.726	5.7	66.7	182.5	15	1.3
55722.93	0.758	0.6	80.8	85.2	3	0.07
55486.71	0.710	22.7	34.4	304.8	15	20.7
55370.92	0.729	2.5	50.5	247.7	10	0.16
<b>CLASSIC</b>						
55794.0	0.762	0.006	72.7	115.3	8	0.02
54672.0	0.852	0.6	55.6	5.0	10	0.20
54406.0	0.928	0.03	86.9	222.6	7	0.01
54301.0	0.827	1.3	56.6	3.0	10	0.28

about 2 seconds of arc, which is well outside our interferometric field of view.

To explore the possibility of an unknown close companion around  $\theta$  Cyg, we performed several tests on our data set. Because the VEGA visibilities are, at first approximation, dominated by one main resolved source, that is the primary component, we adopted a diameter of the companion of 0.2 mas, corresponding to an unresolved source. The UD diameter of the primary was fixed to  $\theta_{\text{UD}} = 0.726$  mas, which is the diameter obtained when merging all nights. Then, by assuming a companion's flux in the range 2% to 15%, we obtained the position angle (PA) and angular separation ( $\rho$ ) corresponding to the minimum  $\chi^2_{\text{reduced}}$ . We performed the same tests with Boyajian et al. (2012)'s CLASSIC data from 2007-2008 (Table 12).

In half of the cases of the VEGA sets, we found a solution with a better  $\chi^2_{\text{reduced}}$  than with a UD model. Generally, the best solution corresponds to a companion with 15% of flux, and a  $\rho$  included between 17.6 and 26.9 mas. However, in the other VEGA cases, the data do fit the binary model and no better solution is found.

In the CLASSIC data, the  $\chi^2_{\text{reduced}}$  is reduced by a factor 2 when we include the binarity. The better UV coverage obtained with the E1S1 baseline provides much better constraints on the model in that case. The best solution for the CLASSIC data gives a flux ratio of about 7% and a separation of about 25 mas. An example of the fit improvement for the CLASSIC measurements is presented in Fig. 6. However, this flux ratio does not permit us to tell which type of star the companion could correspond to, because it is not necessarily bound, but could be either foreground or background.

Finally, we explored the existence of a closure phase signal generated by this close unknown companion (Le Bouquin & Absil 2012). The closure phase is the sum of the phases of the complex visibilities obtained with the three baselines of a triplet. It is independent of the atmosphere, giving direct information of the object's visibility, which results in informations about asymmetries, presence of a companion, etc. We already said that the CLIMB data were at low spatial frequencies due to the longer wavelength of operation. Simulations show that in the baseline configurations used for this paper, the companion will produce a signal lower than 5 or 10 $^\circ$ , which

is below the current accuracy of CLIMB phase closure measurements. However, the simulation shows that a huge closure phase signal of  $\pm 40^\circ$  should be detected by VEGA with the E1E2W2 configuration. Many tests have been performed on the data sets but the signal-to-noise ratio of VEGA phase closure measurements is not sufficient for a correct determination. Unlike from the estimation published in Mourard et al. (2011), we have now a clearer understanding of the noise level in closure phase measurements with VEGA. Closure phase is a third-order moment and the multi-speckle regime of VEGA prevents us from obtaining accurate closure phase measurements for stars fainter than magnitude 1 or 2, depending on seeing conditions (Mourard et al., 2012 in preparation).

## 7. Conclusion

We obtained new and accurate visibility measurements of 14 And,  $\nu$  And and 42 Dra using visible band interferometric observations. From these we derived accurate values of the LD diameter and of fundamental parameters that are fully consistent with those derived with other techniques and bring some improvements in precision. The error bars and  $\chi^2_{\text{reduced}}$  for these three stars are in general much smaller than those obtained on our fourth target :  $\theta$  Cygni. We analyzed the scatter of measurements of  $\theta$  Cyg, taking into account that instrumental or data processing bias are well understood thanks to the good results obtained on the three other stars. It appears that a solution with an unknown companion close to the star helps in reducing the residuals in the model fitting. The limited accuracy in our determination prevents us from being conclusive about the presence of a new close companion around  $\theta$  Cyg, and do not allow us to tell which type of star it could be, because it is not necessarily bound. However, this result encourages organizing new observations in the visible and IR wavelengths, focused on confirming or denying this hypothesis. Closure phase signal is a good way to detect and characterize faint companions around bright stars. We performed simulations of expected closure phase signal for  $\theta$  Cyg with a companion contributing 10% of the flux that is located at 25 mas. As explained before, VEGA is unfortunately not able to measure accurate closure phase signals. CLIMB in K band and MIRC (Monnier et al. 2008) in H band are well-adapted for closure phase tests with the largest CHARA triangle (E1W1S1). Expected signals are presented in Fig. 7. Therefore, a more adequate observing strategy and dedicated observations will be prepared with the combination of the different CHARA beam combiners.

*Acknowledgements.* The CHARA Array is operated with support from the National Science Foundation through grant AST-0908253, the W. M. Keck Foundation, the NASA Exoplanet Science Institute, and from Georgia State University. RL warmly thanks all the VEGA observers that permitted the acquisition of this set of data. RL also acknowledges the PhD financial support from the Observatoire de la Côte d'Azur and the PACA region. We acknowledge the use of the electronic database from CDS, Strasbourg and electronic bibliography maintained by the NASA/ADS system.

## References

- Baines, E. K., Döllinger, M. P., Cusano, F., et al. 2010, ApJ, 710, 1365  
Baines, E. K., McAlister, H. A., ten Brummelaar, T. A., et al. 2009, ApJ, 701, 154  
Baines, E. K., McAlister, H. A., ten Brummelaar, T. A., et al. 2008, ApJ, 680, 728  
Bonneau, D., Clausse, J., Delfosse, X., et al. 2006, A&A, 456, 789  
Born, M., Wolf, E., & Haubold, H. J. 1980, Astronomische Nachrichten, 301, 257  
Boyajian, T. S., McAlister, H. A., van Belle, G., et al. 2012, ApJ, 746, 101

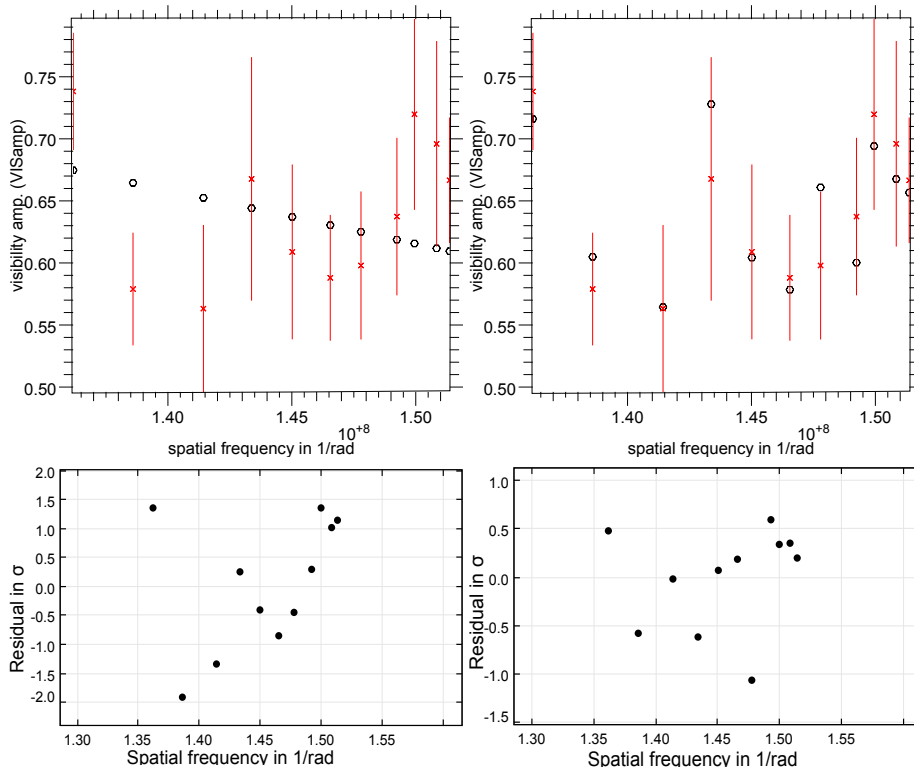


Figure 6: Left column : UD model : right Column : UD model + companion. Top row is for the CLASSIC data visibilities of the RJD 54301 (open circles for the models, crosses for the data), whereas the bottom row corresponds to the visibility residuals.

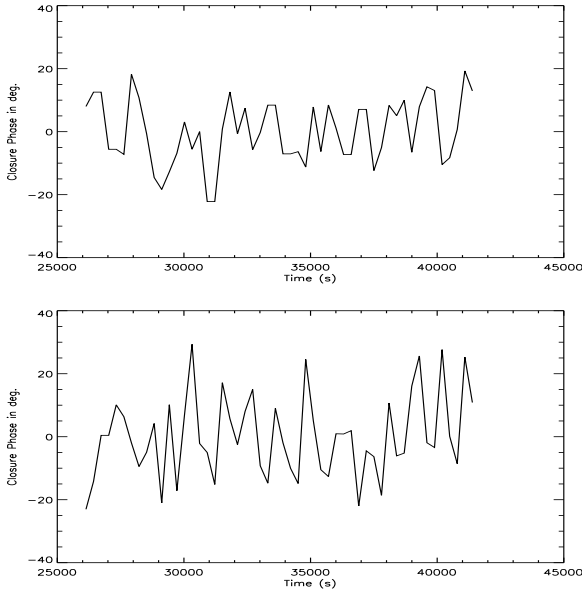


Figure 7: Closure phase signals expected for  $\theta$  Cyg with a companion located at 25 mas that contributes to 10% of the flux. UP : CLIMB in K band, BOTTOM : MIRC in H band. We used the largest triangle of telescopes on CHARA : E1W1S1.

Butler, R. P., Marcy, G. W., Fischer, D. A., et al. 1999, *ApJ*, 526, 916  
 Claret, A. & Bloemen, S. 2011, *A&A*, 529, A75  
 Curiel, S., Cantó, J., Georgiev, L., Chávez, C. E., & Poveda, A. 2011, *A&A*, 525, A78  
 Delfosse, X., Forveille, T., Ségransan, D., et al. 2000, *A&A*, 364, 217  
 Desort, M., Lagrange, A.-M., Galland, F., et al. 2009, *A&A*, 506, 1469

Döllinger, M. P., Hatzes, A. P., Pasquini, L., et al. 2009, *A&A*, 499, 935  
 Erspamer, D. & North, P. 2003, *A&A*, 398, 1121  
 Fuhrmann, K., Pfeiffer, M. J., & Bernkopf, J. 1998, *A&A*, 336, 942  
 Guzik, J. A., Houdek, G., Chaplin, W. J., et al. 2011, *ArXiv e-prints*  
 Guzik, J. A. & Mussack, K. 2010, *ApJ*, 713, 1108  
 Hanbury Brown, R., Davis, J., Lake, R. J. W., & Thompson, R. J. 1974, *MNRAS*, 167, 475  
 Lagrange, A.-M., Desort, M., Galland, F., Udry, S., & Mayor, M. 2009, *A&A*, 495, 335  
 Le Bouquin, J.-B. & Absil, O. 2012, *ArXiv e-prints*  
 Lowrance, P. J., Kirkpatrick, J. D., & Beichman, C. A. 2002, *ApJ*, 572, L79  
 McAlister, H. A., ten Brummelaar, T. A., Gies, D. R., et al. 2005, *ApJ*, 628, 439  
 Monnier, J. D., Zhao, M., Pedretti, E., et al. 2008, in Presented at the Society of Photo-Optical Instrumentation Engineers (SPIE) Conference, Vol. 7013, Society of Photo-Optical Instrumentation Engineers (SPIE) Conference Series  
 Mourard, D., Bério, P., Perraut, K., et al. 2011, *A&A*, 531, A110  
 Mourard, D., Clause, J. M., Marcotto, A., et al. 2009, *A&A*, 508, 1073  
 Roberts, Jr., L. C. 2011, *MNRAS*, 413, 1200  
 Sato, B., Toyota, E., Omiya, M., et al. 2008, *PASJ*, 60, 1317  
 Schneider, J., Dedieu, C., Le Sidaner, P., Savalle, R., & Zolotukhin, I. 2011, *A&A*, 532, A79  
 Sturmman, J., Ten Brummelaar, T., Sturmman, L., & McAlister, H. A. 2010, in Presented at the Society of Photo-Optical Instrumentation Engineers (SPIE) Conference, Vol. 7734, Society of Photo-Optical Instrumentation Engineers (SPIE) Conference Series  
 Tallon-Bosc, I., Tallon, M., Thiébaud, E., et al. 2008, in Society of Photo-Optical Instrumentation Engineers (SPIE) Conference Series, Vol. 7013, Society of Photo-Optical Instrumentation Engineers (SPIE) Conference Series  
 ten Brummelaar, T. A., McAlister, H. A., Ridgway, S. T., et al. 2005, *ApJ*, 628, 453  
 Tkachenko, A., Lehmann, H., Smalley, B., Deboscher, J., & Aerts, C. 2012, *ArXiv e-prints*  
 van Belle, G. T., van Belle, G., Creech-Eakman, M. J., et al. 2008, *ApJS*, 176, 276  
 van Belle, G. T. & von Braun, K. 2009, *ApJ*, 694, 1085  
 van Leeuwen, F. 2007, *A&A*, 474, 653  
 von Braun, K., Boyajian, T. S., ten Brummelaar, T. A., et al. 2011, *ApJ*, 740, 49  
 Wright, J. T., Upadhyay, S., Marcy, G. W., et al. 2009, *ApJ*, 693, 1084

## Appendix A: Individual angular diameter determinations

We present here the different individual LD angular diameter determinations for the various epochs of observation of  $\theta$  Cygni. The individual LD diameters are given in Tab. 11.

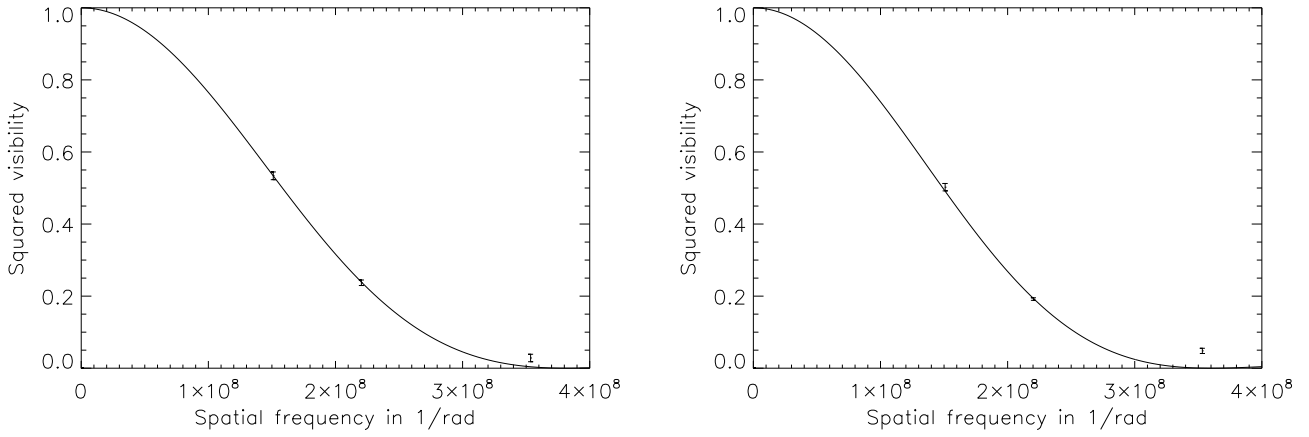


Figure A.1: Model of squared visibility for the RJD 55849.62 (left,  $\theta_{LD} = 0.700 \pm 0.011$ ) and 55848.62 (right,  $\theta_{LD} = 0.744 \pm 0.007$ ) obtained by LITpro.

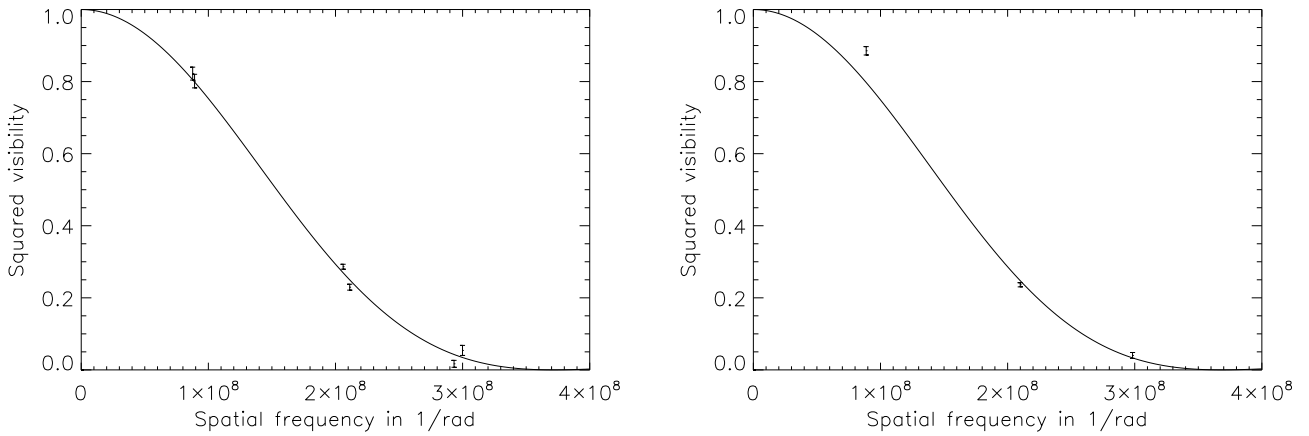


Figure A.2: Model of squared visibility for the RJD 55826.67 (left,  $\theta_{LD} = 0.721 \pm 0.009$ ) and 55805.75 (right,  $\theta_{LD} = 0.727 \pm 0.010$ ) obtained by LITpro.

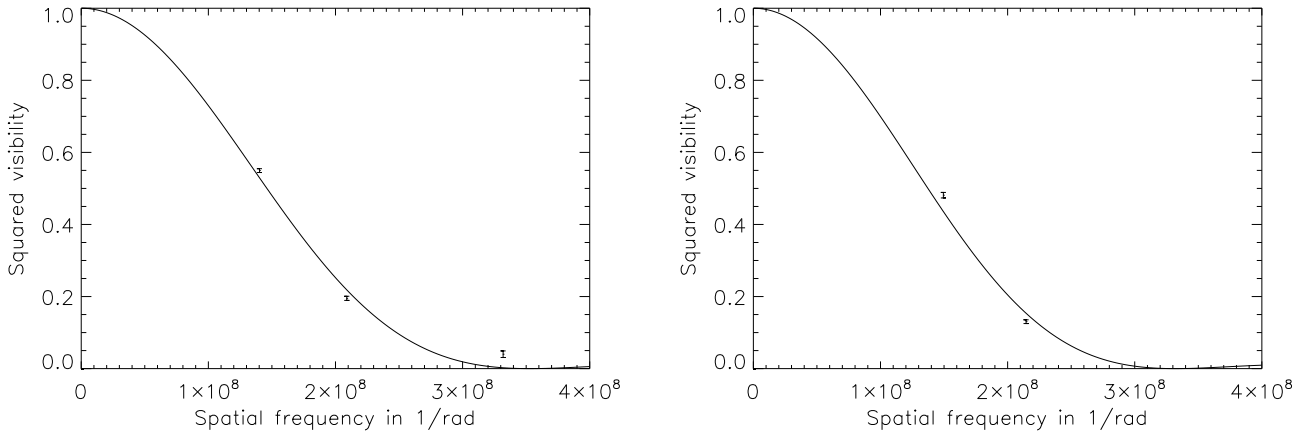


Figure A.3: Model of squared visibility for the RJD 55803.77 (left,  $\theta_{LD} = 0.759 \pm 0.008$ ) and 55774.73 (right,  $\theta_{LD} = 0.807 \pm 0.010$ ) obtained by LITpro.

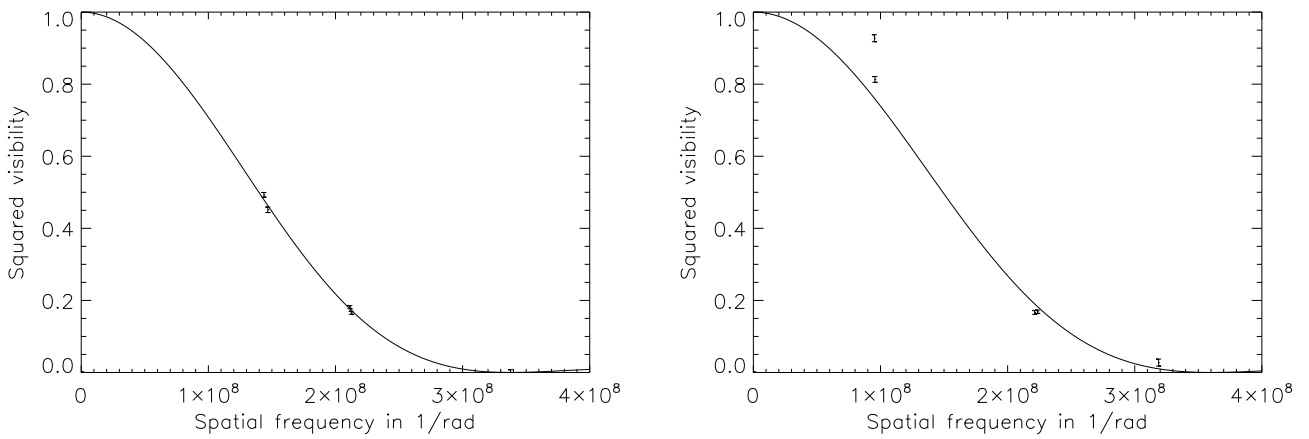


Figure A.4: Model of squared visibility for the RJD 55722.93 (left,  $\theta_{LD} = 0.793 \pm 0.006$ ) and 55486.71 (right,  $\theta_{LD} = 0.744 \pm 0.007$ ) obtained by LITpro.

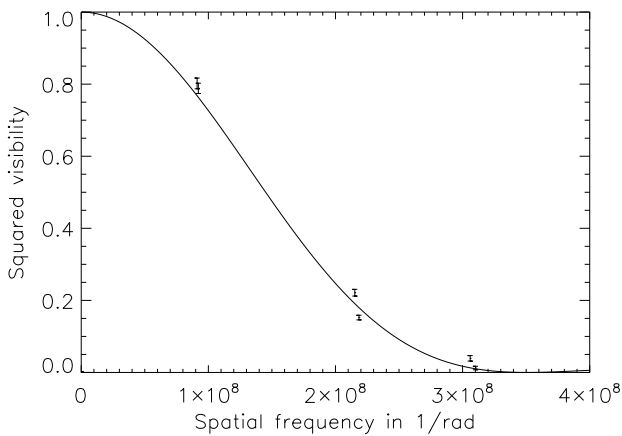


Figure A.5: Model of squared visibility for the RJD 55370.92 ( $\theta_{LD} = 0.764 \pm 0.010$ ) obtained by LITpro.